Uplink Array Calibration via Far-Field Power Maximization

V. Vilnrotter,[1] R. Mukai,[1] and D. Lee[1]

Uplink antenna arrays have the potential to greatly increase the Deep Space Network's high-data-rate uplink capabilities as well as useful range, and to provide additional uplink signal power during critical spacecraft emergencies. While techniques for calibrating an array of receive antennas have been addressed previously, proven concepts for uplink array calibration have yet to be demonstrated. This article describes a method of utilizing the Moon as a natural far-field reflector for calibrating a phased array of uplink antennas. Using this calibration technique, the radio frequency carriers transmitted by each antenna of the array are optimally phased to ensure that the uplink power received by the spacecraft is maximized.

I. Introduction

Uplink arraying is a fundamentally new concept that promises to dramatically increase NASA's future deep-space communications capabilities. The requirements to command spacecraft after launch and during encounter, and to provide two-way communication and two-way ranging as well as in-flight reconfiguration to accommodate changes to mission objectives, are integral parts of every deep-space mission. The use of antenna arrays enables greater data rates, greater effective operating distance, and cost-effective scaling for more demanding future missions through a highly flexible design philosophy, via the inherently parallel architecture of antenna arrays.

Currently, uplink command and telemetry functions are carried out by 34- and 70-meter antennas in the Deep Space Network (DSN). The newer 34-meter antennas are used for routine uplink operations, whereas the older 70-meter antennas are employed when greater range or data rate is required. However, the 70-meter antennas may soon be decommissioned due to age and increasing maintenance costs. Instead of building new 70-meter-aperture or larger antennas, current plans call for the construction of arrays of smaller antennas together with the required signal processing to maintain and eventually greatly surpass NASA's long-range and high-data-rate communications capabilities.

The current uplink capabilities of a long-range 70-meter antenna, equipped with a 20-kW X-band transmitter, can be maintained by configuring two existing 34-meter antennas (also with 20-kW transmitters) as a two-element uplink array. Adding more 34-meter antennas to the two-element uplink array continues to improve on current 70-meter uplink capabilities since the far-field power increases as the square of the number of antennas when the transmitter power on each antenna remains the same. It is

[1] Communications Architectures and Research Section.

The research described in this publication was carried out by the Jet Propulsion Laboratory, California Institute of Technology, under a contract with the National Aeronautics and Space Administration.

anticipated that either new 34-meter antennas will be built in the future to provide even greater uplink capabilities or large numbers of smaller antennas will be constructed and configured as uplink arrays to meet future requirements via cost-effective and flexible array architectures.

The use of arrays for uplink applications requires precise knowledge of the phase vector that maximizes the power density along the desired line of sight (LOS) towards the spacecraft. Initially, the phase vector of the array must be calibrated with sufficient accuracy along the calibration LOS, after which the calibration vector has to be translated to the spacecraft LOS and maintained dynamically throughout the track. This article addresses the first of these requirements, namely the initial calibration of the array vector via far-field radar calibration.

II. Uplink Array System Model

A functional block diagram of a two-element uplink array constructed using the existing 34-meter beam-waveguide (BWG) antennas at the Goldstone Deep Space Communications Complex (GDSCC) is shown in Fig. 1. The antennas in this block diagram are located at the Apollo Deep Space Station (DSS) 24 and DSS 25, where initial Moon-bounce experiments already have been carried out, but also could include the 34-meter antenna at DSS 26 in future experiments. The intent is to identify and characterize the key components of an experimental two-element uplink array system that will be used to demonstrate the calibration algorithms described in this article.

Critical to any array for which precision measurements of phase are required is an accurate and stable reference frequency subsystem that can be used to determine the phase of each antenna at a specified

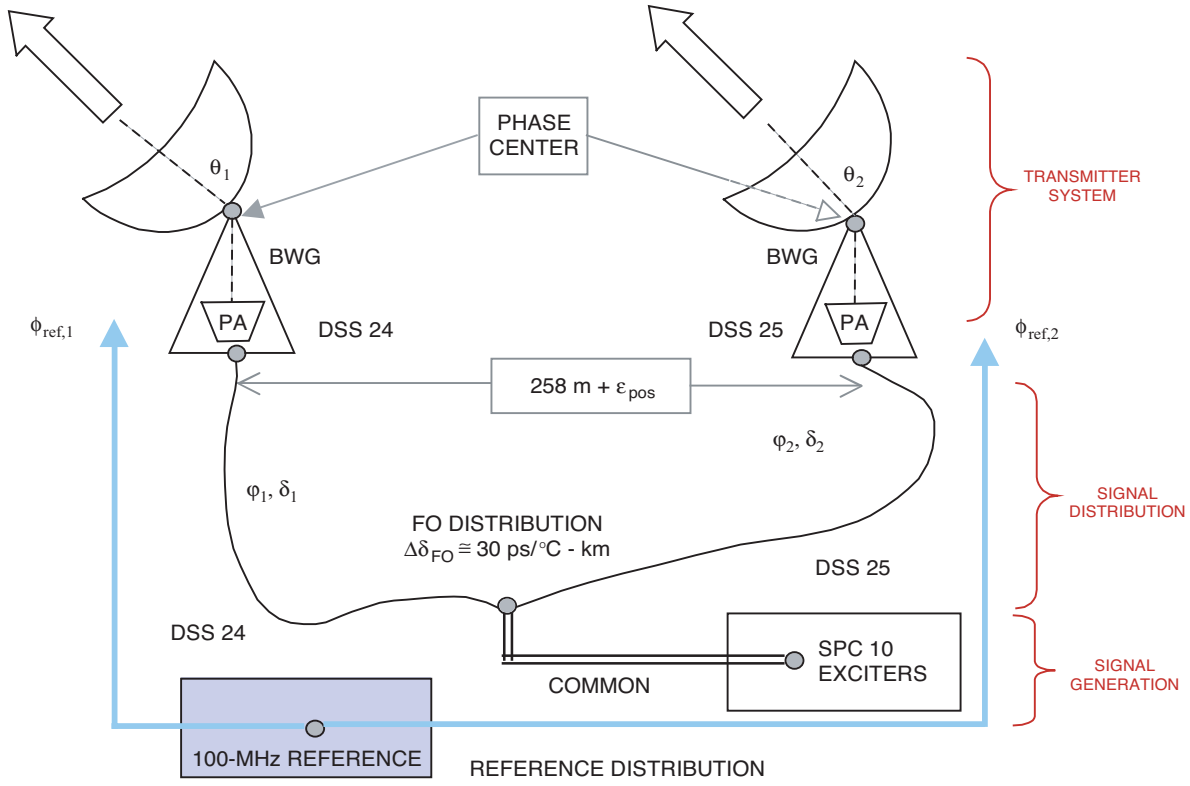

Fig. 1. Conceptual diagram of a two-element uplink array, identifying reference frequency generation and distribution, signal distribution, power amplifiers (PAs), and antenna phase centers.

point in the electronic signal path. The highest (hence most accurate) reference frequency distributed at the GDSCC is 100 MHz, with a differential stability between co-located antennas on the order of a few hertz per day. Such an accurate reference frequency enables differential comparison of the transmitted carrier phase up to a day after initial calibration, reducing the frequency of calibrations between uplink transmissions.

The carrier frequency envisioned for operational uplink arraying is X-band 7.1- to 7.9-GHz, which is the current uplink frequency, well separated from the nominal 8.4-GHz downlink carrier frequency. At these X-band frequencies, tropospheric delay variations do not present a serious problem under nominal operating conditions, but could be measured along the antenna LOS and incorporated into the calibration vector using standard water vapor radiometer (WVR) techniques, if required. In this article, we do not consider tropospheric effects on the uplink signal, but refer the interested reader to previous articles that treat this subject in detail [1,2].

The X-band signals are generated at the central Signal Processing Center (SPC) 10 located at DSS 14 and distributed via fiber to the Apollo complex where the antennas are located, some 16 kilometers away. The exciters generating the X-band carriers also impose modulation on the signal on demand and have the capability to incorporate predict-based differential Doppler compensation to cancel the effects of Earth rotation on the transmitted carriers. The compensated X-band carriers are amplified by 20-kW power amplifiers located in the pedestal room of the BWG antennas. Finally, the amplified X-band fields are launched into space in the commanded pointing direction via the beam-waveguide interface.

Studies addressing the stability of the phase centers of the three-antenna cluster at the Apollo station indicate that differential drift between antennas is on the order of a millimeter over several years,[2] which translates to about 10 degrees of electrical phase at the X-band uplink carrier frequency, implying that differential drift in phase centers between uplink array calibration is not a significant problem. The antenna phase center, defined as the intersection of the azimuth and elevation axes, is a convenient point for referencing the phase of the X-band carrier at each antenna: the antenna phases θ_i in the following theoretical development are understood to be measured at the phase center of each antenna.

III. Far-Field Calibration Principles and Algorithms

The far-field calibration techniques covered in this section do not include the case when a spacecraft downlink signal is available, since uplink calibration may be required even when a downlink signal is not available. Therefore, we restrict our attention to calibration techniques that rely on natural sources or radar reflectors that are visible at least once a day, such as quasars and the Moon. Two distinct calibration scenarios will be considered: calibration by measuring the interferometric phase, obtained either from a natural point source such as a quasar or from an illuminated target such as the Moon, and applicable to both uplink and downlink arrays; and calibration via a novel far-field power maximization scheme developed specifically for uplink arrays.

Uplink array calibration is defined as the process of obtaining the phase vector required to project a maximally narrow beam in the direction of a spacecraft or other target, with accuracy exceeding the angular dimensions of the far-field beam. The key concepts required for understanding array calibration, and in particular uplink array calibration, can be defined and illustrated by considering the calibration of a two-element array in receive mode via a distant point source, such as a compact quasar.

A. Receive-Mode Calibration Using Quasar Radiation

Quasars are a natural source of strong radio frequency (RF) radiation, and their spatial extent generally is small compared to the beamwidth of the antenna elements or even to the secondary beam of a compact

[2] C. Jacobs, personal communication, Jet Propulsion Laboratory, Pasadena, California, 2005.

array. The signal it generates appears as white noise over receiver bandwidths of interest (50 to 100 MHz); hence, the radiation from a noise-like point source can be modeled as a plane wave with random, wideband modulation.

As shown in Fig. 2, the downconverted complex baseband signal received by two antennas with a geometrical range difference of $R_2 - R_1$ is of the form

$$s_i(t) = n_Q\left(t - \frac{R_i}{c}\right)\exp\left[j\left(\frac{2\pi R_i}{\lambda} + \theta_i\right)\right] \tag{1}$$

where λ is the carrier wavelength, c is the speed of light, and θ_i, $i = 1, 2$ is the instrument phase associated with antenna "i" in receive mode. These signals are observed in the presence of additive noise; however, we do not consider additive noise in this article, instead relegating it to a future article in which the performance of uplink array calibration algorithms will be addressed.

The quasar signal shown in Fig. 2 is wideband and hence can be assumed to be delta-correlated for large receiver bandwidths. Therefore, applying the delay difference to one of the signals and correlating the delay-compensated received waveforms from the two antennas yields the expected value:

$$\begin{aligned} &E\left\{\frac{1}{T}\int_0^T s_1\left(t - \frac{R_2 - R_1}{c}\right)s_2^*(t)\,dt\right\} \\ &\quad = \frac{1}{T}\exp\left[j\left(\frac{2\pi(R_2 - R_1)}{\lambda} + \theta_2 - \theta_1\right) + \right]\int_0^T E\left\{n_Q\left(t - \frac{R_2}{c}\right)n_Q^*\left(t - \frac{R_2}{c}\right)\right\}dt \\ &\quad = \sigma_Q^2\exp\left[j\left(\frac{2\pi(R_2 - R_1)}{\lambda} + \theta_2 - \theta_1\right)\right] \end{aligned} \tag{2}$$

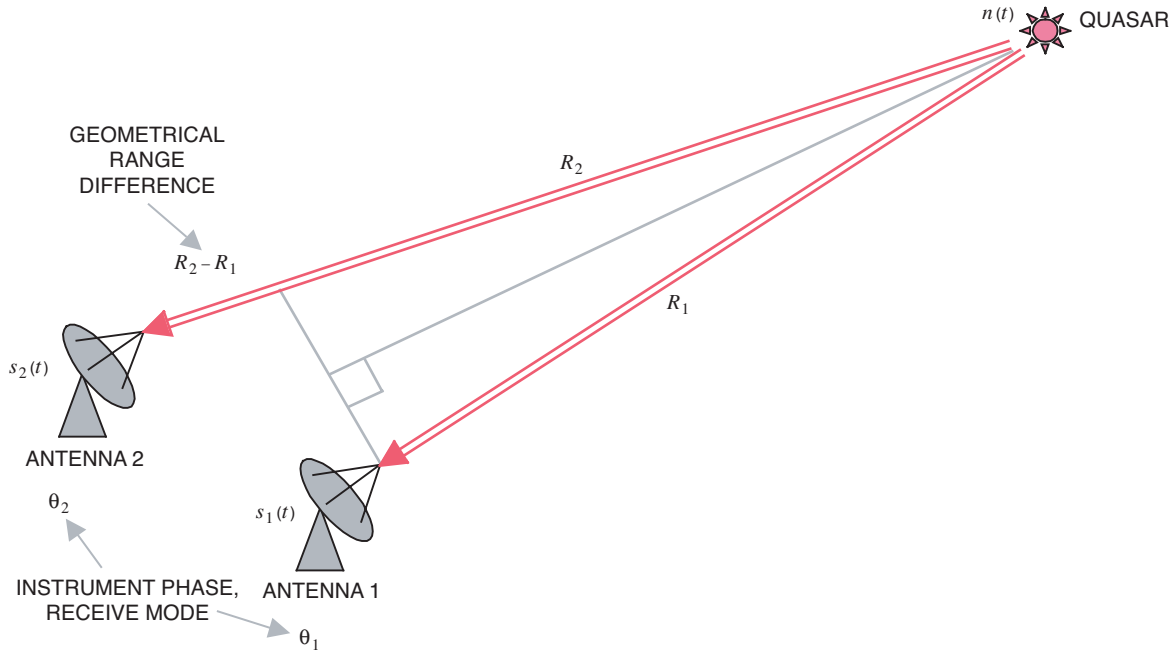

Fig. 2. Array and source geometry for calibrating two antennas using a distant point source, such as a quasar.

where $\sigma_Q^2 = E|n_Q^2(t)|$ is the variance of the noise-like point-source or, equivalently, the power of the received quasar signal. The interferometric phase is an estimate of the geometric phase difference plus the difference of the receive-mode instrument phases. It can be recovered from the correlation by taking the arc-tangent of the ratio of the imaginary and real components. If the geometric phase difference is known precisely, then it can be subtracted from the interferometric phase, leaving an estimate of the difference of the instrument phases needed to calibrate the antenna pair.

B. Receive-Mode Calibration Using Interferometric Synthetic Apperture Radar Techniques

The concept of extracting interferometric phase between two receive antennas using a distant point source can be extended to radiation reflected from rough surfaces, such as the surface of the Moon [3].[3] If the lunar surface is illuminated by radio waves, the reflected components can be detected on the ground by sensitive receivers and processed to extract the phase information. Consider a portion of the lunar surface illuminated by radio waves as in Fig. 3. The reflected component just above the surface is the result of reflections by a multitude of scatterers at different distances and can be represented by a complex field distribution.

The impinging radio wave $s(t)$ is taken to be a plane wave. After encountering the rough surface, a portion of the signal field is reflected, with some fraction of the total reflected power propagating back towards the transmitter. Since the scatterers are at slightly different distances, the phase of each reflected component tends to be random, but stationary for a short time. A hypothetical plane just above the lunar surface is convenient for analyzing the return signal for the purpose of developing a two-dimensional model. This model then is applied to analyze the Moon-bounce calibration algorithms.

Consider the Cartesian coordinate system attached to the virtual plane just above the lunar surface, as shown in Fig. 3. We can model the reflected fields as the product of a nominal return plane wave and an amplitude and phase distortion function, $h(x, y)$. Define the spatial coherence function H as the expectation of the product of displaced distortion functions:

$$H(x_1 - x_2, y_1 - y_2) \equiv E\{h(x_1, y_1)h^*(x_2, y_2)\} \tag{3}$$

where the expectation is over the ensemble of independent surface samples from a given region. This coherence function can be used to generate a complete set of orthonormal functions that are useful for expanding the random reflected fields. The eigenfunctions of the coherence kernel, $\xi(x, y)$, satisfy the integral equation:

$$\iint dx_1 dy_1 H(x_1 - x_2, y_1 - y_2)\xi_j(x_1, y_1) = \varsigma_j \xi_j(x_2, y_2) \tag{4}$$

where ς_j is the eigenvalue associated with the jth eigenfunction, $\xi_j(x, y)$. The reflected field, $r(x, y; t)$, can be expanded in terms of these functions as $r(x, y; t) = \sum_j r_j(t)\xi_j(x, y)$, where $E\{r_j(t)r_k^*(t)\} = \rho_j(t)\delta_{jk}$ and $\rho_j = |h_j|^2$; in other words, the spatial coefficients are uncorrelated. Expansions of this type, that make use of the eigenfunctions of the coherence kernel, are known as Karhounen–Loeve (K-L) expansions and are used extensively in communications theory and signal processing to generate expansions with uncorrelated (or, in the case of Gaussian processes, independent) coefficients. For isotropic coherence kernels, these eigenfunctions are often peaked, unimodal functions, leading to a spatial sampling interpretation for the K-L expansion. This interpretation effectively replaces the continuous lunar surface with a sampled representation, incorporating the complex reflection coefficient in the neighborhood of each sample into the expansion coefficients. This sampled model is illustrated in Fig. 4, where several scattering coefficients

[3] F. Wang and K. Sarabandi, *Study of Uplink Large Array Calibration Using In-Orbit Targets*, Progress Report III (internal document), University of Michigan, April 2005.

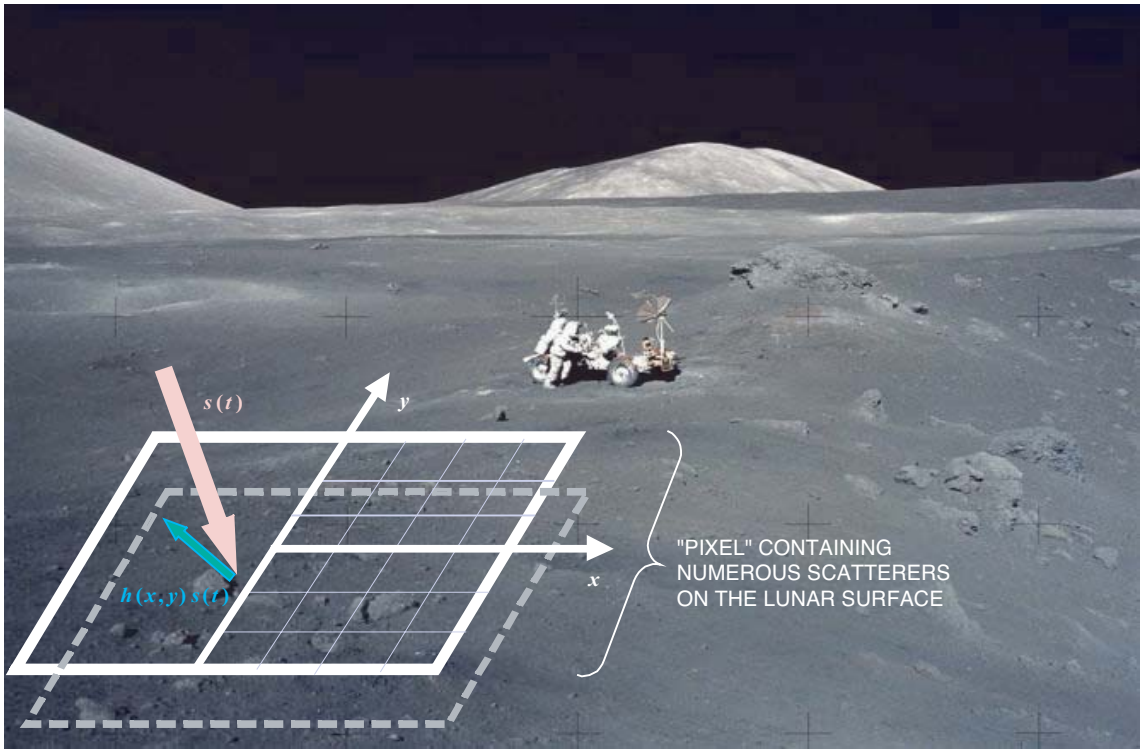

Fig. 3. Example of lunar surface illuminated by the signal and the reflected component.

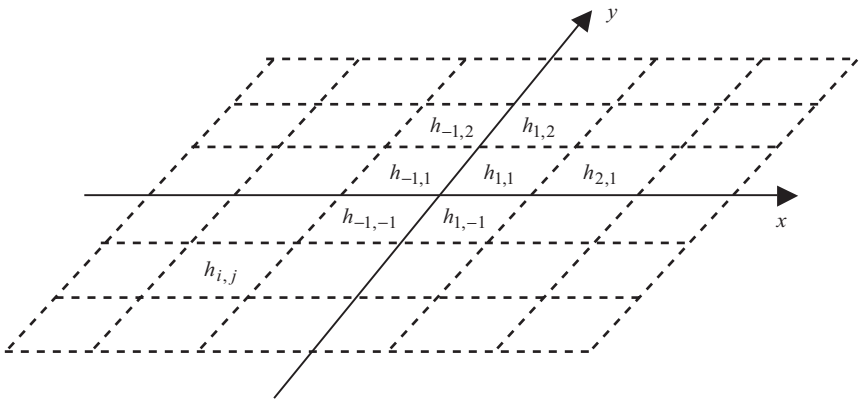

Fig. 4. Illustration of complex reflection coefficients for the sampling interpretation.

are identified. For convenience, we shall refer the scattered power ρ to the receiving antenna, in effect absorbing the propagation loss from the Earth to the Moon into the coefficients.

It is well-known[4] [3] that the lunar surface imparts different Doppler shifts to radio signals reflected from thin "slices" parallel to the apparent spin axis. In addition, the near-spherical mean surface of the Moon can be decomposed into concentric rings of equal distance, or delay, from the receivers, radiating outwards from the apparent center of the Moon. The intersection of the Doppler slices and concentric delay rings gives rise to "pixels" on the lunar surface with distinct Doppler-delay signatures, as illustrated in Fig. 5.

[4] Ibid.

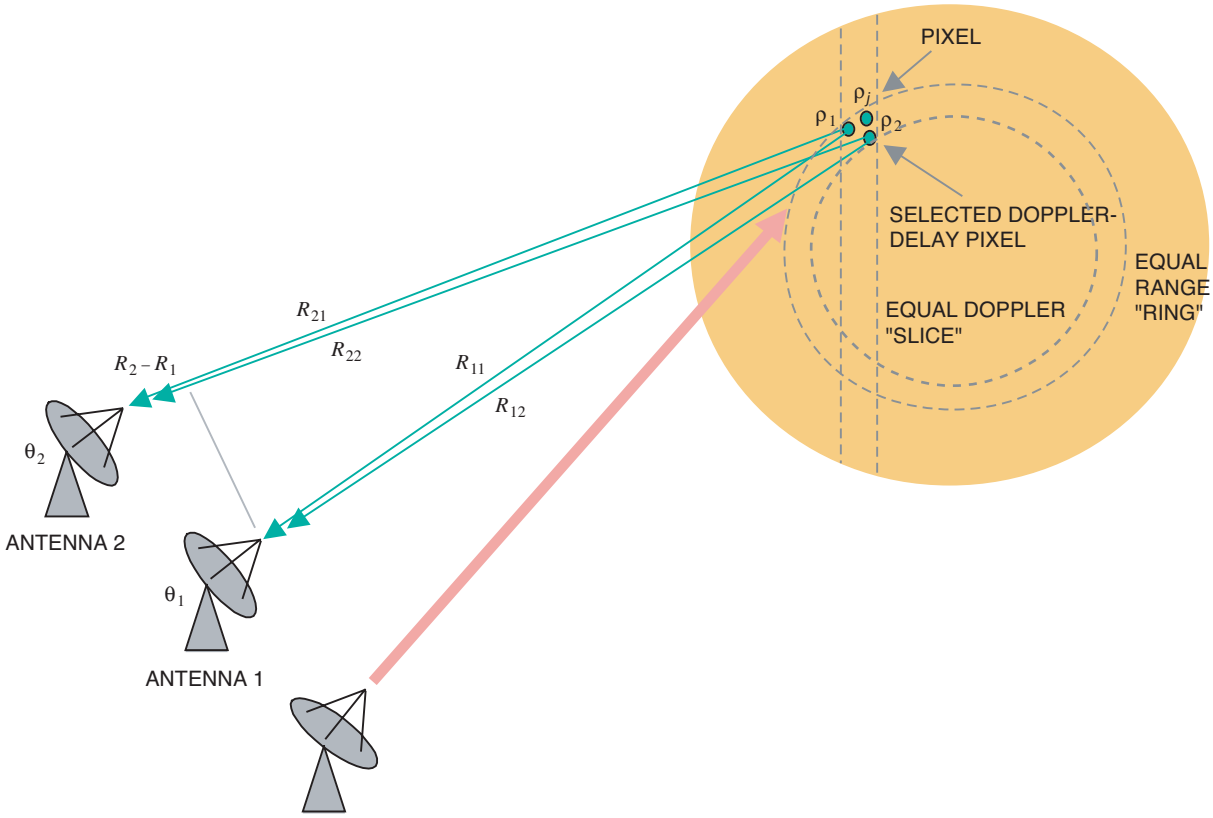

Fig. 5. Receive mode uplink array calibration using interferometric SAR, illustrating the Doppler-delay technique.

With a single antenna transmitting and two antennas receiving, a Doppler-delay pixel on the lunar surface can be isolated through the use of a matched filter at each antenna, designed to respond only to signal components with specific range and Doppler parameters. Range resolution can be obtained by modulating the transmitted signal with a pseudorandom noise (PN) code whose autocorrelation function peaks at the desired delay; Doppler resolution can be achieved by filtering out all but a narrow band of frequencies around the desired Doppler frequency. A transmitted illuminating signal incorporating these features and, therefore, enabling the matched filtering operation at the receivers is of the form $x(t) = m(t)\exp[j(\omega t)]$, where $m(t)$ is a PN sequence with chip duration and total range designed to provide the desired range resolution and to simultaneously eliminate range ambiguity. The carrier frequency is arbitrary but known to the receivers, enabling computation of the desired Doppler slice a priori.

The Doppler-delay pixel typically extends over hundreds of meters to kilometers and hence contains a great many sample coefficients. To simplify notation, we assume that the scattering coefficients have been renumbered using a single index, j, instead of the two indices (i, j) shown in Fig. 4. With P watts illuminating the selected pixel, the complex envelope of the scattered component received by the ith antenna on the ground, due to the jth scatterer within this pixel, is of the form

$$r_{ij}(t) = \sqrt{P} h_j m\left(t - \frac{R_{ij}}{c}\right) \exp\left[j\left(\omega_{ij} t + \frac{2\pi R_{ij}}{\lambda} + \theta_i\right)\right] \tag{5}$$

where h_j is the complex coefficient of the scattered signal component received at the ith antenna (after propagation losses have been taken into account), λ is the carrier wavelength, R_{ij} is the total pathlength from the jth scatterer to the ith antenna, and θ_i is the instrumental phase associated with the ith receiver.

Using a single subscript to identify the scatterers within the desired Doppler-delay pixel, the total signal received from the Moon within the design range and Doppler slice of the matched filter can be expressed as

$$r_i(t) = \sum_j \sqrt{P} h_j m\left(t - \frac{R_{ij}}{c}\right) \exp\left[j\left(\omega_{ij} t + \frac{2\pi R_{ij}}{\lambda} + \theta_i\right)\right]$$

$$\cong \sqrt{P} m\left(t - \frac{\bar{R}_i}{c}\right) \exp\left[j\left(\bar{\omega}_i t + \frac{2\pi \bar{R}_i}{\lambda} + \theta_i\right)\right] \sum_j h_j \tag{6}$$

where $\bar{R}_i$ and $\bar{\omega}_i$ are the average range and Doppler frequency of the desired pixel, observed at the ith receiving antenna. Performing the correlation of the signals from two antennas and taking the expected value yields

$$E\left\{\int_0^T r_1\left(t - \frac{\bar{R}_2 - \bar{R}_1}{c}\right) r_2^*(t)\, dt\right\}$$

$$= E\int_0^T \left\{m^2\left(t - \frac{\bar{R}_2}{c}\right) \exp\left[-j\left(\frac{2\pi(\bar{R}_2 - \bar{R}_1)}{\lambda} + (\theta_2 - \theta_1)\right)\right] \sum_j P|h_j|^2 + \text{crossterms}\right\} dt$$

$$= P \exp\left[-j\left(\frac{2\pi(\bar{R}_2 - \bar{R}_1)}{\lambda} + (\theta_2 - \theta_1)\right)\right] \sum_j \rho_j = PN\bar{\rho} \exp\left[-j\left(\frac{2\pi(\bar{R}_2 - \bar{R}_1)}{\lambda} + (\theta_2 - \theta_1)\right)\right] \tag{7}$$

Equation (7) shows that the interferometric phase can be recovered from a pixel on the lunar surface, in general comprised of a large number of scatterers. In effect, we can view the pixel as an average scattering surface with reflection coefficient $\beta = N\bar{\rho}/A_{\text{pixel}}$. This interpretation is helpful for estimating the received power, given the illuminating power density and the size of the Doppler-delay pixel.

C. Direct Uplink Array Calibration Using "Moon-Bounce" Power Maximization

The calibration techniques described above rely on receive-mode calibration of two antennas, whereby the signal is received simultaneously either from a distant point source (quasar) or from a pre-selected Doppler-delay pixel on the lunar surface, illuminated from the ground. These techniques are applicable to cases for which a receiver is available on the uplink antennas, and in addition the received phase can be accurately translated to the uplink transmitter system. If a downlink signal from the spacecraft were available, and if the calibration between the receiver and transmitter sections of the uplink antennas could be characterized and preserved, then the downlink signal itself could be used to calibrate the uplink array. However, in the general case when no downlink signal is available due to spacecraft malfunction or other operational constraints, this method of calibration may not be available during routine operational scenarios.

A preferred method for calibrating the uplink array is in transmit mode, where all of the array elements are transmitting towards a predetermined point in space and where the far-field signal power is maximized in the desired look direction through a direct far-field measurement. The same mathematical concepts developed in the above receive-mode calibration approaches can be employed to develop the new concepts required for transmit-mode calibration of the uplink array. For transmit-mode calibration, it is necessary to take into account the relative delay and differential Doppler between the two transmitting antennas.

The geometrical relationship between the two transmitting antennas and a single receiver antenna designed to receive signal power only from the pre-selected Doppler-delay pixel is shown in Fig. 6. The range difference between the two antennas is $R_2 - R_1$, which gives rise to a delay difference of $(R_2 - R_1)/c$ in the modulation and to a total phase difference of $2\pi(R_2 - R_1)/\lambda$ in the carrier phase. Taking these offsets into account, the transmitted signals from the two antennas would arrive at the lunar surface in phase and with compensated delay if the instrument phases θ_1 and θ_2 were equal. However, even if the instrumental phases are not equal at the array elements, there is a point in the primary illumination pattern where the phases are exactly equal, guaranteed by the fact that the separation of the antenna centers always exceeds the antenna diameter.

Denoting the delay and Doppler compensated signals leaving the two antennas by $x_1(t)$ and $x_2(t)$,

$$\begin{aligned} x_1(t) &= \sqrt{P_t} m_t(t) \exp\left[j(\omega t + \theta_1)\right] \\ x_2(t) &= \sqrt{P_t} m_t\left(t - \frac{R_2 - R_1}{c}\right) \exp\left[j\left(\omega t + \frac{2\pi(R_2 - R_1)}{\lambda} + \theta_2\right)\right] \end{aligned} \tag{8}$$

where $m_t(t)$ refers to the transmitted modulation. The sum of the transmitted signals impinging on the lunar surface is of the form $x(t) = C[x_1(t) + x_2(t)] = Cm(t)\exp(j\omega t)[\exp(j\theta_1) + \exp(j\theta_2)]$, where C is

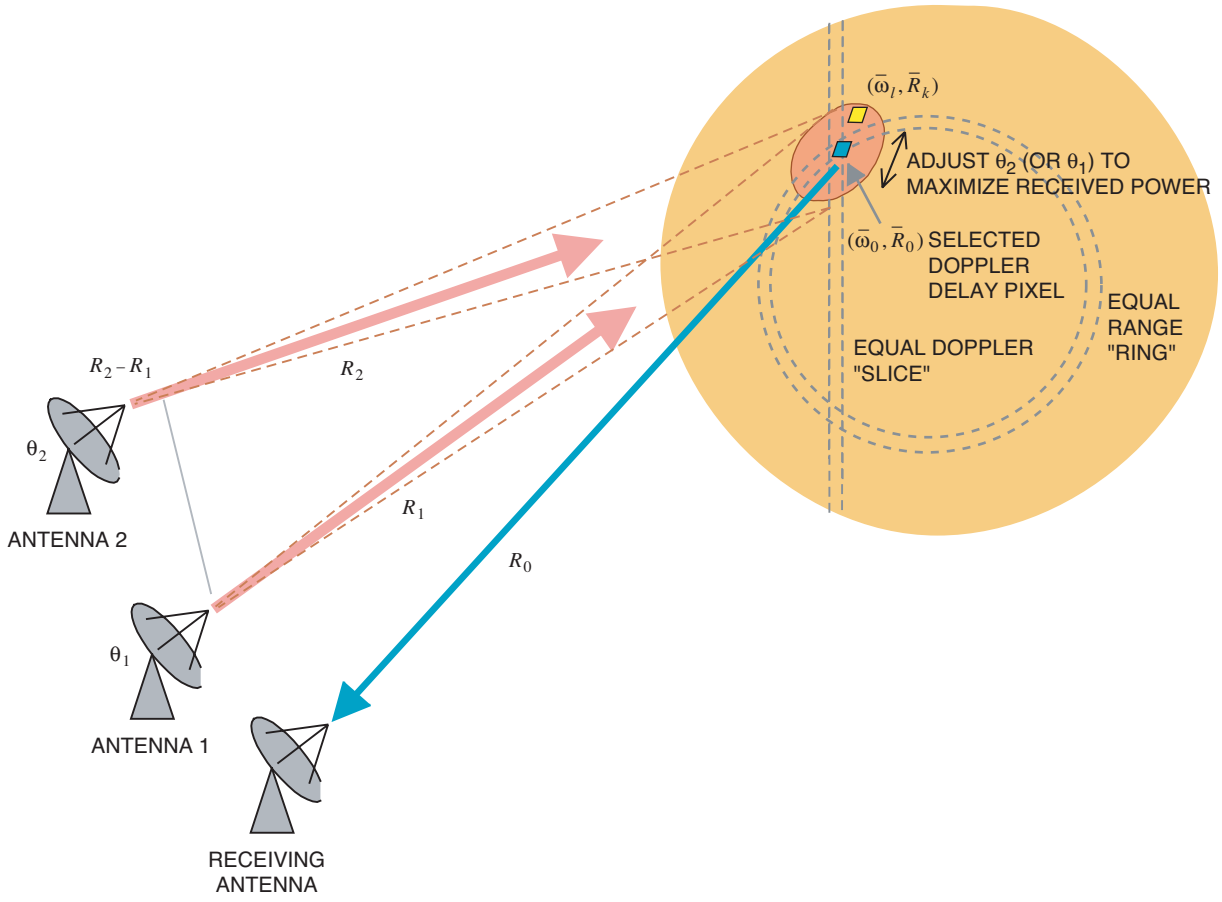

Fig. 6. Transmit mode uplink array calibration, illustrating electronic scanning of the far-field signal distribution by varying the differential antenna phase.

a constant coefficient. Consider the point over the lunar surface where $\theta_1 = \theta_2$. Absorbing the complex constant into the coefficient, we can see that the amplitude of the illuminating field at this point on the surface is twice the field magnitude; hence, the power is proportional to four times the power from each antenna. At a point where the phase of the second (or first) antenna differs from that of the first (or second) antenna by π radians, the two exponentials cancel, and the power over that point on the lunar surface is reduced to zero. It is clear that, for any point on the lunar surface within the overlapping footprint of the two antennas, the phases could be made to add or cancel by varying the phase of one of the antennas on the ground, resulting in constructive or destructive interference at a given point in the far field. Varying the phase of one antenna to scan the peak of the interference pattern over a line formed by the projection of the antenna baseline onto the center of the antenna footprint in this manner amounts to a form of electronic beamsteering in the far field of the array. We incorporate this concept into our model by defining the constant coefficient as $C = 2\sqrt{P_t(\Delta\theta)} \rightarrow 2\sqrt{P_t}$, with $\Delta\theta \equiv \theta_2 - \theta_1$ and the understanding that P_t is a function of the phase difference. It is clear that the arrayed power can be alternately maximized and nulled over the point on the surface where $\theta_1 = \theta_2$ by adding and removing π radians to θ_1 (or θ_2) on the ground.

After encountering the lunar surface, a Doppler frequency generated by an effective lunar spin is added to the carrier frequency of the reflected components. We assume that each reflecting surface within the selected pixel has approximately the same relative radial velocity, and approximately the same range, as any other. Adjacent pixels, on the other hand, have different rotational velocities, or range, or both, from the selected pixel. Denoting the average Doppler-shifted carrier frequency and average range of the selected pixel by $(\bar{\omega}_0, \bar{R}_0)$, respectively, and that of the kl-th pixel by $(\bar{\omega}_k, \bar{R}_l)$, and assigning a random complex reflection coefficient $h_{kl}(n)$ to the nth reflecting surface within the kl-th pixel, the received signal from the klth pixel contains all reflected components from that pixel and is of the form

$$r_{kl}(t) = m\left(t - \frac{\bar{R}_k}{c}\right)\exp(j\bar{\omega}_l t)\sum_n h_{kl}(n) \tag{9}$$

where propagation losses and ground antenna gain have been incorporated into the complex coefficients $h_{kl}(n)$. Assuming that the receiving antenna is of the same diameter as the transmitting antennas, it collects reflections from all pixels within the illuminated footprint, yielding the total received signal $r(t) = \sum_{k,l} r_{kl}(t)$. The reflections from the selected pixel can be isolated by correlating the received signal with a PN sequence and Doppler frequency matched to the Doppler-delay signature of the selected pixel. Denoting this function by $m(t - [\bar{R}_0/c])\exp(-j\bar{\omega}_0 t)$, the result of the correlation operation is

$$\begin{aligned}
&\frac{1}{T}\int_0^T r(t) m\left(t - \frac{\bar{R}_0}{c}\right)\exp(-j\bar{\omega}_0 t)\,dt \\
&\quad = \frac{1}{T}\int_0^T \{r_{00}(t) + r_{01}(t) + \cdots + r_{kl}(t) + \cdots\}\, m\left(t - \frac{\bar{R}_0}{c}\right)\exp(-j\bar{\omega}_0 t)\,dt = 2\sqrt{P_t}\sum_n h_{00}(n) \\
&\qquad + \frac{1}{T}\int_0^T \left\{\cdots + 2\sqrt{P_t}\sum_n h_{kl}(n) m\left(t - \frac{\bar{R}_l}{c}\right) m\left(t - \frac{\bar{R}_0}{c}\right)\exp[-j(\bar{\omega}_k - \bar{\omega}_0)t] + \cdots\right\} dt \\
&= 2\sqrt{P_t}\sum_n h_{00}(n) + (\text{terms close to zero}) \cong 2\sqrt{P_t}\sum_{\text{n}} h_{00}(n)
\end{aligned} \tag{10}$$

In other words, only those scattered components originating from the selected pixel survive the correlation operation; all other reflected components are eliminated by virtue of the fact that the autocorrelation of

the PN sequence is zero (or very close to zero) for all integer shifts, and that integrals of the complex exponential function over an integer number of cycles are zero. The integration time T should be at least as long as the PN sequence and, further, it should be selected so as to make sure that correlations over adjacent pixels are close to zero.

Equation (10) shows that the correlation operation eliminates the scattered signal field components from all but the selected pixel. Taking the expected value of the squared magnitude of the correlation yields the average reflected power collected by the receiver:

$$4P_tE\left|\sum_n h_{00}(n)\right|^2 = 4P_tE\left(\sum_n\sum_m h_{00}(n)h_{00}^*(m)\right)$$

$$= 4P_t\sum_n E|h_{00}(n)|^2 + 4P_t\sum_n\sum_{\substack{m\\ n\neq m}} E\,h_{00}(n)h_{00}^*(m) = 4P_t\sum_n \rho_n \qquad (11)$$

When the interference pattern generated by the antenna pair reaches its peak over the selected pixel, the received power in the matched filter is maximized for any realization of the scattering surfaces, resulting in a 6-dB gain in reflected power over a single transmitting antenna. Higher average bulk reflectivity, characterized by larger average ρ_n within the selected pixel, yields higher average received power; therefore, it is advantageous to search for regions of high reflectivity at the carrier frequency of interest. Next, we turn to the problem of maximizing the received power in a systematic way by varying the phase between two antennas on the ground, and then extend these concepts to the general case of a large number of transmitting antennas.

IV. "Moon-Bounce" Calibration of Uplink Arrays

Two distinct algorithms for maximizing the power of an uplink array in a given look direction will be considered. First, we describe our methodology for maximizing the received power for a two-antenna uplink array by varying the relative phases of the antennas in a systematic fashion and making measurements of the reflected signal amplitude, and then we extend this technique to 2^L antennas by repeated application of the two-pair algorithm. Second, a gradient ascent algorithm will be described that has been developed for optical phase retrieval applications in adaptive optics systems [3], but which has been modified for calibrating large radio frequency uplink arrays.

A. Maximizing Uplink Power in the Case of a Two-Antenna Array

In the far field, the beam pattern of a single antenna is given by the Fourier transform of the field distribution over the antenna aperture. If the pupil function is assumed to be an ideal circular pupil function, the pattern is that given by Goodman [5]:

$$\frac{R\cdot\exp\left(j\frac{k}{2f}\rho^2\right)}{j\rho}J_1\left(\frac{2\pi\rho R}{\lambda f}\right)$$

where R is the antenna radius in meters, f is the distance to the target, and k is the wave number $2\pi/\lambda$. We are using the polar coordinates (ρ,ϕ) to describe points in the target plane. An example of the simulated far field of a single 34-meter antenna located 3.84×10^5 kilometers from the target plane (at the distance of the Moon) is shown in Fig. 7.

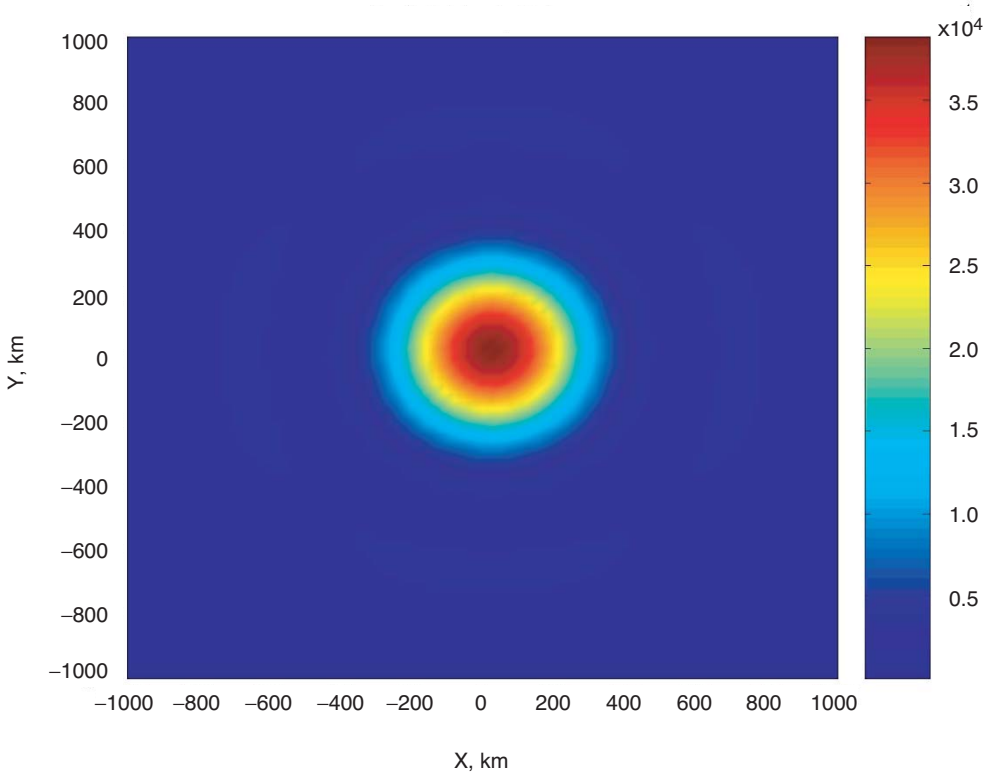

Fig. 7. Single-antenna transmitted far-field intensity pattern.

When two antennas are arrayed, the far-field distribution is now the Fourier transform of the aperture function of the two-element array. A two-element array can be viewed as the convolution of the antenna pupil function with two impulses located at the phase center of each array; hence, in the Fourier transform domain, this yields the product of the antenna far-field pattern and a sinusoidal interference pattern characteristic of Young's well-known experiment. This compound intensity pattern is shown in Fig. 8.

We can maximize the received power at a point P in the far field using the following algorithm. Let $\theta_1(0)$ denote the original phase of antenna 1, and let $\theta_2(0)$ denote the original phase of antenna 2. Let the phase of the two antennas as a function of integer time increment n, denoting the nth sample, be given by $\theta_1(n)$ and $\theta_2(n)$, respectively, and apply the following differential modulation scheme:

(1) Let $\theta_1(n) = \theta_1(0)$ throughout the maximization.

(2) Let $\theta_2(n) = \theta_2(0) + \left[\frac{2\pi n}{N_r}\right] + \frac{[1+(-1)^n]}{2}\pi$, where $N_r \gg 1$.

In other words, we apply a phase ramp from 0 to 2π radians with period N_r and simultaneously add an alternating phase term of π radians of much higher repetition rate to the phase ramp. Since the addition of π radians interchanges the peak of the pattern with a null, the above procedure effectively toggles the peak of the far-field array pattern on and off the nominal array LOS, thus yielding a differential measurement of the reflected power from the desired target point. The receiver observes both a sinusoidal variation in the power as a function of the phase ramp being applied and a rapidly alternating term, where the difference in the amplitudes of the alternating term is proportional to the received signal level. The point of maximum difference in the received power can be taken as the point where the phases $\theta_1(n)$ and $\theta_2(n)$ are equal.

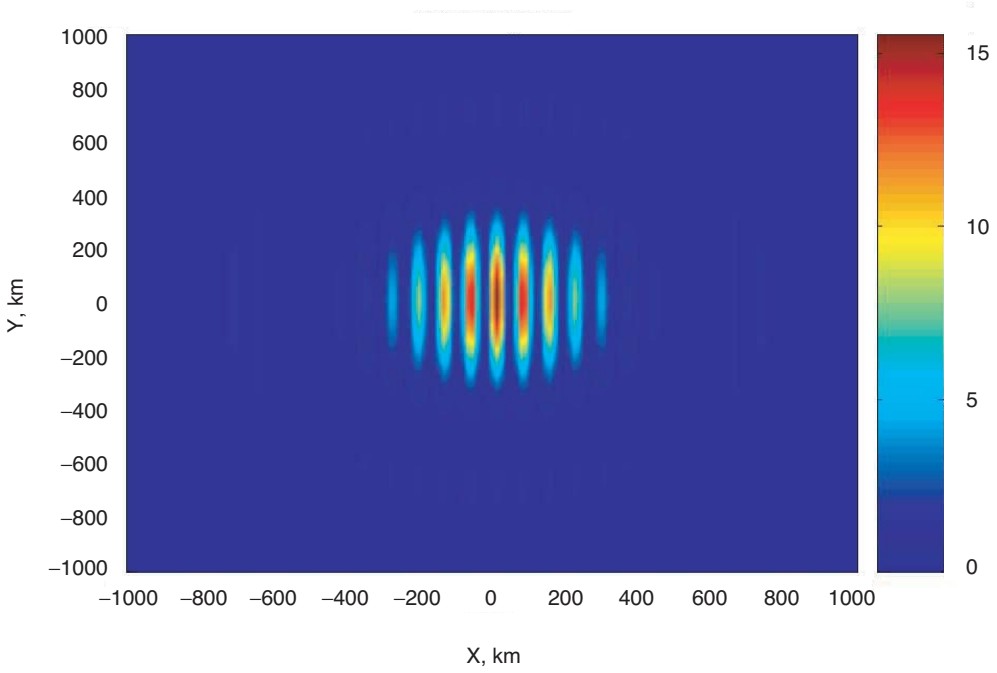

Fig. 8. Dual-antenna transmitted far-field intensity pattern.

Utilizing the above maximization procedure, the received power as a function of time is shown in Fig. 9. Here the blue/red lines denote power with and without the rapid π radian phase term applied. As the difference in received power with and without the π radian phase shift increases, the line remains blue until the maximum difference is reached (the power difference is shown as a black line). Once this maximum is reached, the blue lines change to red, and we continue measuring power differences. The phase at which the maximum power difference occurs is the "calibration phase" that aligns the phase of antenna 2 with that of antenna 1.

B. Maximizing Received Power with $M = 2^L$ Antennas

Here we assume the transmitted RF carriers can be modulated using suitable orthogonal PN codes as necessary to distinguish between different antenna pairs. The use of such codes makes it possible to maximize the power of a given pair of antennas, using the procedure described in the previous section, while ignoring the reflected signal from other antenna pairs. For example, if antennas 1 and 2 use PN code 1 while antennas 3 and 4 use PN code 2, then the uplink power at the target point for antennas 1 and 2 can be maximized independently of the other pair by virtue of the orthogonality of the PN codes.

It is now possible to align antenna phases pairwise in the array if orthogonal PN codes are used; hence, we can align the phases of 2^L antennas as follows:

(1) Divide the set of 2^L antennas into 2^{L-1} pairs of antennas.

(2) Maximize the uplink power at the target point for each of the 2^{L-1} antenna pairs. This can be done in parallel due to the orthogonality of the PN sequences being used.

(3) After performing step (2) above, treat each of the 2^{L-1} antenna pairs as a single antenna. Then repeat this process by pairing up the 2^{L-1} "antennas" to form 2^{L-2} "antenna pairs" and repeat the process.

The total number of steps required is only L, making this a logarithmic time procedure in the number of antennas.

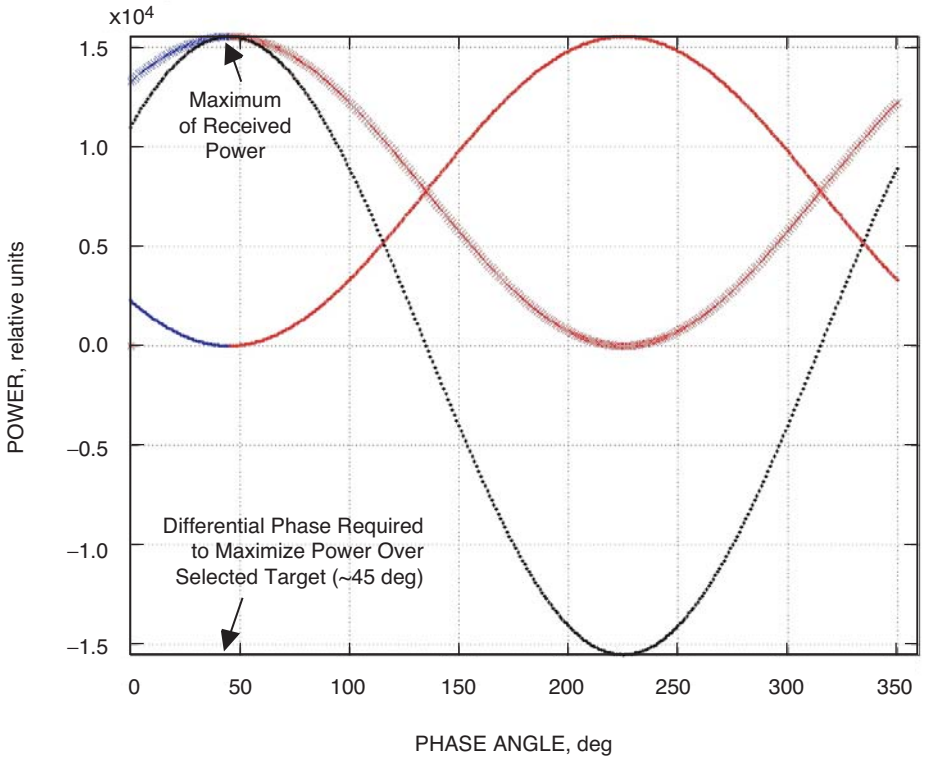

Fig. 9. Example of power maximization as a function of applied differential phase.

C. Gradient Ascent Calibration Algorithm

Another candidate algorithm for power maximization is gradient ascent. Let M denote the number of antennas, and let their phases as a function of sample time n be given in the phase vector $\mathbf{x}(n) = \begin{bmatrix}\theta_1(n) & \theta_2(n) & \cdots & \theta_M(n)\end{bmatrix}$. The gradient ascent procedure works as follows [4]:

(1) Apply a set of phase perturbations given by $\delta\mathbf{x}(n) = \begin{bmatrix}\delta\theta_1(n) & \delta\theta_2(n) & \cdots & \delta\theta_M(n)\end{bmatrix}$.

(2) Measure the change in received power: δP.

(3) Update the phase vector via the recursive algorithm: $\mathbf{x}(n+1) = \mathbf{x}(n) + \alpha \cdot \delta P \cdot \delta\mathbf{x}(n)$.

This procedure was shown by Carhart et al. [6] to work very well for maximizing received power in the focal plane, using only intensity measurements. Since both the far-field Fraunhofer diffraction pattern and the focal-plane field pattern are given by a Fourier transform relationship [5] and since Carhart et al. were performing cost function minimization in the focal plane of their system, the algorithm developed by Carhart applies as much to far-field problems as it does to the focal-plane problem. Therefore, this technique provides an alternate method for phasing up an uplink array consisting of more than two elements.

V. Summary and Conclusions

We have presented three different approaches to far-field calibration of uplink arrays. The first array calibration method utilizes a distant radio source (e.g., a quasar) to determine the interferometric phase between the two antennas in receive mode. The difference in the receive mode instrument phase of the two antennas then is derived by subtracting correction factors due to geometry and atmosphere from

the measured interferometric phase. Assuming that transmit and receive chains in each antenna share a common path, the calibrated delay in receive mode can, in principle, be translated to delay in transmit mode. This method has the advantage that it is based on VLBI techniques well-established in the deep-space community. However, uplink array calibration may be problematic with this technique for an array of small antenna elements because available quasars may be too weak a signal source to provide sufficient SNR, and because phase variations in transmit chain elements not common to the receiving chain (e.g., high-power amplifier, exciter) may cause drift in the transmitter delay relative to the measured receiver delay.

The second calibration technique addresses the SNR problem by measuring reflected power from a closer target in the far-field (namely the Moon). This is accomplished by using a single transmit antenna to "bounce" a modulated PN sequence off the Moon, and correlating the received return signal at two different antennas. Because of the large number of scatterers on the Moon (which cannot be modeled as a point source), it is necessary to isolate reflections from a particular segment of the lunar surface using Doppler-delay techniques. However, this calibration method also has the disadvantage of employing a measurement of the receive mode phase—hence, the transmitter phase may be subject to drift.

The third calibration technique addresses both problems encountered in the previous methods by using the uplink array in transmit mode. With this technique, the phase of the first transmit antenna is held constant while the phase of the second transmitter is varied, and the uplink array is calibrated by maximizing the received reflected power. As with the second calibration method, delay-Doppler pixels are used to isolate reflections from a small portion of the lunar surface. The applicability of these techniques to practical operational uplink array calibration will be determined by means of additional analysis, simulation, and experiments. Uplink array calibration experiments involving the 34-meter BWG antennas at the Goldstone complex are the subject of current research and will be described in a future article.

References

[1] S. J. Keihm, "Water Vapor Radiometer Measurements of the Tropospheric Delay Fluctuations at Goldstone Over a Full Year," *The Telecommunications and Data Acquisition Progress Report 42-122, April–June 1995*, Jet Propulsion Laboratory, Pasadena, California, pp. 1–11, August 15, 1995. http://ipnpr/progress_report/42-122/122J.pdf

[2] S. J. Keihm, A. Tanner, and H. Rosenberger, "Measurements and Calibration of Tropospheric Delay at Goldstone from the Cassini Media Calibration System," *The Interplanetary Network Progress Report*, vol. 42-158, Jet Propulsion Laboratory, Pasadena, California, pp. 1–17, August 15, 2004. http://ipnpr/progress_report/42-158/158A.pdf

[3] J.-L. Margot, D. B. Campbell, R. F. Jurgens, and M. A. Slade, "Digital Elevation Models of the Moon from Earth-Based Radar Interferometry," *IEEE Transactions on Geoscience and Remote Sensing*, vol. 38, no. 2, pp. 1122–1133, March 2000.

[4] R. Mukai, K. Wilson, and V. Vilnrotter, "Application of Genetic and Gradient Descent Algorithms to Wavefront Compensation for Deep-Space Optical Communications," *The Interplanetary Network Progress Report*, vol. 42-161, Jet Propulsion Laboratory, Pasadena, California, pp. 1–21, May 15, 2005. http://ipnpr/progress_report/42-161/161U.pdf

[5] J. W. Goodman, *Introduction to Fourier Optics*, 2nd. ed., Boston, Massachusetts: McGraw-Hill, 1996.

[6] G. W. Carhart, J. C. Ricklin, V. P. Sivokon, and M. A. Vorontsov, "Parallel Perturbation Gradient Descent Algorithm for Adaptive Wavefront Correction," *Proceedings of the SPIE*, San Diego, California, pp. 221–227, 1997.